Phase-resolved Spectroscopy and Photometry of the Eclipsing Polar, UZ Fornacis

Z.N Khangale[1,2], S.B Potter[1], P.A Woudt[2]

1. South African Astronomical Observatory, P.O. Box 9, 7935 Observatory, South Africa
2. Department of Astronomy, University of Cape Town, Private Bag X3, Rondebosch 7701, South Africa

Correspondence: khangalezn@saao.ac.za

ABSTRACT

We present high-speed photometry and phase-resolved spectroscopy of the eclipsing polar UZ Fornacis. The blue continuum of UZ For is dominated by single- or double-peaked emission from the HeII, HeI and the Balmer lines. The red spectrum shows weak emission from NaI doublet at 8183 Å and 8194 Å and strong emission from CaII lines at 8498 Å and 8542 Å. Doppler tomography, using the inside-out technique based on the fast maximum entropy, of the strongest features reveal the presence of emission from the threading region, the ballistic and magnetic confined accretion stream as well as the irradiated face of the secondary star. We have obtained 28 new eclipse times of UZ For to test the two-planet model proposed to explain variations in its eclipse times. The new data agree with the predicted model but requires the outer planet to be highly eccentric. The new orbital periods for the inner and outer planets are 5.17(2) and 14.76(3) years, respectively.

INTRODUCTION

Polars are a sub-class of cataclysmic variable (CVs) stars in which the white dwarf is strongly magnetic. The presence of the magnetic field prevents the formation of an accretion disc. UZ Fornacis (here after UZ For) is an eclipsing polar discovered with the EXOSAT as an X-ray source, EXO 033319-2554.2 (Giommi et al., 1987). It has an orbital period of ∼126.5 min and has been studied extensively on a wide range of wavelengths including optical, x-ray and polarimetry. UZ For display one or two accretion spots depending on the accretion state, with magnetic fields of ∼53 and ∼48 MG. Recently, Potter et al. (2011) conducted a high-speed multi-instrument photometry and precisely measuring the mid-time eclipse aimed at detecting variations in the orbital period of UZ For. Their results reveal a departure from linear to quadratic trend of ∼60 s. The departure suggests two cyclic variations of 16(3) and 5.25(25) years. The two favoured mechanism to derive the periodicities are either two giant extrasolar planets as companion to the binary or magnetic cycle mechanism of the secondary star.

OBSERVATIONS

Photometry and photo-polarimetry observations of UZ For were made with the SAAO 1.9-m telescope using the Sutherland High-speed Optical Camera (SHOC; Gulbis et al. 2011; Coppejans et al. 2013) and the HIgh-speed Photo-POlarimeter (HiPPO; Potter et al. 2010). A total of 28 high-time resolution and high S/N ratio eclipses of the target were observed from which measurements were made.

Spectroscopic observations were made with the Southern African Large Telescope (SALT; Buckley et al. 2006) using the Robert-Stobbie Spectrograph (RSS; Burgh et al., 2003; Kobulnicky et al., 2003). A long-slit of width 1.5″ was used and a total of 23 (blue) and 14 (red) medium resolution spectra, with 360 s exposure, and a wavelength coverage of ∼4050-5100Å and ∼7550-8650Å. The data was reduced using PYSALT and IRAF routines.

RESULTS

Eclipse Time Variations

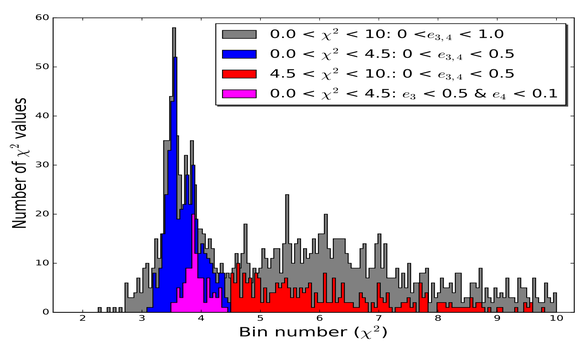

Figure 1: The distribution of the reduced χ^2 parameter space for the fitting parameter. The colors are explained in the legend.

Potter et al. (2011) used Equ. 1 to describe Observed minus Calculated eclipse time variations of UZ For:

$$T(BJD_{TDB}) = T_0 + P_{bin}E + AE^2 + K_{bin,(3)}sin(\upsilon_3 - \varpi_3)\frac{[1-e_3^2]}{[1+e_3cos(\upsilon_3)]} + K_{bin,(4)}sin(\upsilon_4 - \varpi_4)\frac{[1-e_4^2]}{[1+e_4cos(\upsilon_4)]}, \quad (1)$$

where T_0 - epoch, P_{bin} - orbital period, and A - the quadratic parameter. The remaining five free parameters are the orbital parameters of the two extra bodies. $e_{(3,4)}$ are the eccentricities of the two bodies. To investigate the 13 dimensional parameter space we generated a grid of 10000 × 13 starting parameters and used the **Least-Square** fit to find the final solutions – all the 13 parameters were allowed to vary. The final 10000 fits had a reduced χ^2 with distribution shown in Fig. 1. It's clear that most solutions are clustered around $0 \leq \chi^2 \leq 4.5$. We chose our best solutions based on the reduced χ^2 and the eccentricity values as follows:

- first, we explored the solutions with $3.0 \leq \chi^2 \leq 4.5$ and $0.0 \leq e_{(3,4)} \leq 0.5$ (marked in blue, Fig. 1),
- then chose solutions with $0.0 \leq e_4 \leq 0.1$ and $3.0 \leq \chi^2 \leq 4.5$ for the inner planet (marked in margenta, Fig. 1).

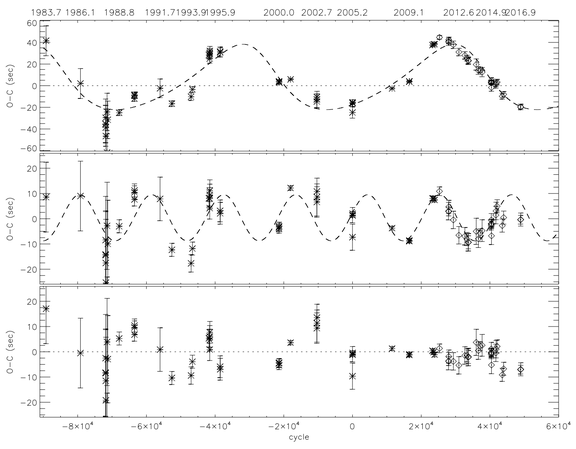

Figure 2: The O-C diagram of UZ For after successive subtraction of the three terms constructed using the fitting parameters obtained using all the eclipse times of UZ For, with the new data included the fitting.

The updated O–C diagram (Fig. 2) is consistent with earlier conclusions from Potter et al. 2011 of the presence of two cyclic variations of 5.25(25) and 16(3) years. The refined two cyclic variations are 5.17(2) and 14.76(3) years, respectively. In our case the outer planet is required to have eccentricity of 0.4-0.5, but it is difficult to conceive stable orbits of such high eccentricity. The inner planet's eccentricity is consistent with zero ($e_4 \leq 0.1$). The solution overplotted in Fig. 2 is the best mathematical fit to the data and also a representation of all solutions with $0.0 \leq e_4 \leq 0.1$ and $3.0 \leq \chi^2 \leq 4.5$. The new eclipses agree with the predictions and the two cyclic variations are well within the uncertainty of the solution presented in Potter et al. 2011. The cyclic variations may be due to the presence of the two planets or some form of Applegate's (Applegate, 1992) mechanism working in UZ For.

Spectral Analysis

Phase-resolved spectroscopy of CVs allows us to study variations in emission or absorption lines in the binary system as the two stars orbit each other around their center of mass. This also allows one to measure radial velocity and mapping of their emitting region in velocity space in the form of Doppler tomography.

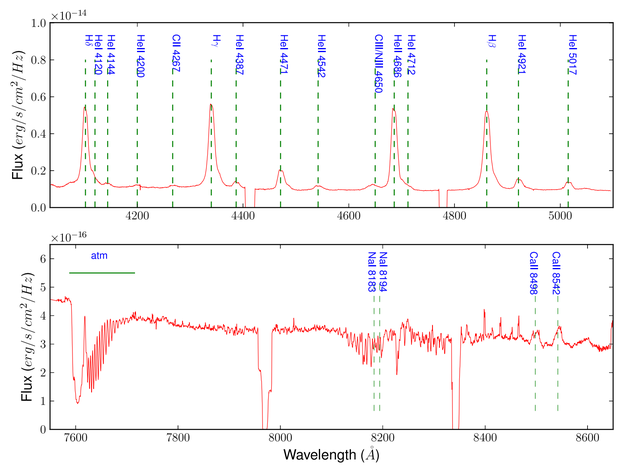

Figure 3: The average wavelength calibrated blue (top) and red (bottom) spectra of UZ For obtained with SALT. Prominent emission or absorption features has been labeled.

Figure 3 (top panel) shows the average blue spectrum:

- dominated by single- and/or double-peaked emission from the Balmer lines, HeII and HeI lines,
- other lines: the Bowen blend (CIII/NIII at 4650Å) and CII 4267Å, all appears in weak emission.

The red spectrum, Fig. 3 (bottom panel):

- show weak absorption from NaI at 8183 Å and 8194 Å
- and also strong emission from the CaII lines at 8498 Å and 8542Å.

We used the strongest features e.g. HeII 4686 and HI lines, from both the blue spectra to compute Doppler maps of emission lines for further investigation.

Modulation Flux Doppler Mapping

Doppler tomography is an indirect imaging technique developed by Marsh & Horne (1988) in which orbitally phase-resolved spectra are used to reconstruct a two-dimensional image in velocity space of the emission distribution in interacting binaries. We performed Doppler tomography of the strongest emission lines using the inside-out technique developed by Kotze et al. (2015), this reverses the standard velocity projection by transposing the zero-velocity origin to the outer circumference and the maximum velocities to origin of the velocity space. The inside-out technique uses polar coordinates (Kotze et al., 2015).. We have over-plotted a model with the WD mass, M_1 = 0.3 $M_\odot$, the mass ratio $q = \frac{M_2}{M_1}$ = 0.25 and inclination i = 81°.

Trailed Spectra

The observed trailed spectra show three distinct components:

- a relatively narrow component with low amplitude and associated with the irradiated face of the secondary,
- the broad emission component (blue) with high velocity amplitude, and the broad feature (yellow) which is visible throughout the orbital phase. These are produced from various parts of the accretion flow.

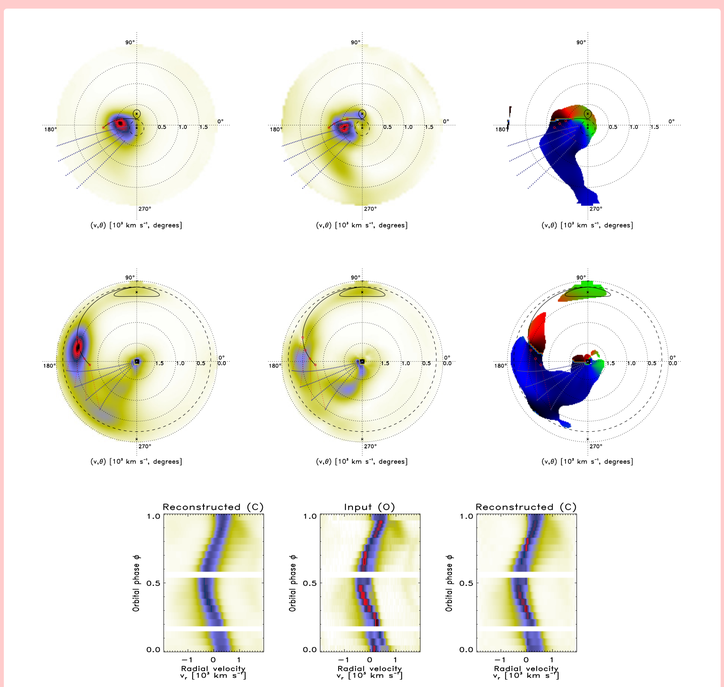

Figure 4: Standard (top row) and inside-out (middle row) Doppler tomography: average map, modulation amplitude and phase of maximum flux maps; and the observed and reconstructed trailed spectra for HeII 4686Å.

Doppler Maps

1. Both the standard and inside-out average Doppler maps:
   - emission dominated by the threading region,
   - show emission from the irradiated face of secondary star,
   - and emission from the ballistic and magnetically confined accretion stream.
2. The modulation amplitude maps show that the ballistic and magnetic confined stream are the most flux modulated components. The flux of the secondary star is also shown to modulate.
3. Doppler map of phase of maximum flux show which component of the binary is visible. The secondary star is seen around ϕ = 0.5, when the irradiated face is pointing towards the observer.

The inside-out technique better exposes the low-velocity emission details which are overly compacted in the standard tomograms. This is apparent in most of features discussed above are more pronounced in the inside-out Doppler maps.

Summary

- We have investigated the eclipse time variations of UZ For – our solution is consistent with the two periods reported in Potter et al. (2011).
- We have presented both the standard and inside-out Doppler tomography of UZ For to investigate its accretion dynamics.

Acknowledgments

This material is based upon work supported financially by the National Research Foundation. Any opinions, findings and conclusions or recommendations expressed in this material are those of the the author(s) and therefore the NRF does not accept any liability in regard thereto.

References

Applegate, J. H. 1992, ApJ, 385, 621

Buckley, D. A. H., Burgh, E. B., Cottrell, P. L., Nordsieck, K. H., O'Donoghue, D., & Williams, T. B. 2006, in Proc. SPIE, Vol. 6269, Society of Photo-Optical Instrumentation Engineers (SPIE) Conference Series, 62690A

Burgh, E. B., Nordsieck, K. H., Kobulnicky, H. A., Williams, T. B., O'Donoghue, D., Smith, M. P., & Percival, J. W. 2003, in Proc. SPIE, Vol. 4841, Instrument Design and Performance for Optical/Infrared Ground-based Telescopes, ed. M. Iye & A. F. M. Moorwood, 1463–1471

Coppejans, R., Gulbis, A. A. S., Kotze, M. M., Coppejans, D. L., Worters, H. L., Woudt, P. A., Whittal, H., Cloete, J., & Fourie, P. 2013, PASP, 125, 976

Giommi, P., Angelini, L., Osborne, J., Stella, L., Tagliaferri, G., Beuermann, K., & Thomas, H.-C. 1987, IAU Circ., 4486, 1

Gulbis, A. A. S., O'Donoghue, D., Fourie, P., Rust, M., Sass, C., & Stoffels, J. 2011, in EPSC-DPS Joint Meeting 2011, 1173

Kobulnicky, H. A., Nordsieck, K. H., Burgh, E. B., Smith, M. P., Percival, J. W., Williams, T. B., & O'Donoghue, D. 2003, in Proc. SPIE, Vol. 4841, Instrument Design and Performance for Optical/Infrared Ground-based Telescopes, ed. M. Iye & A. F. M. Moorwood, 1634–1644

Kotze, E. J., Potter, S. B., & McBride, V. A. 2015, A&A, 579, A77

Marsh, T. R. & Horne, K. 1988, MNRAS, 235, 269

Potter, S. B., Buckley, D. A. H., O'Donoghue, D., Romero-Colmenero, E., O'Connor, J., Fourie, P., Evans, G., Sass, C., Crause, L., Still, M., Butters, O. W., Norton, A. J., & Mukai, K. 2010, MNRAS, 402, 1161

Potter, S. B., Romero-Colmenero, E., Ramsay, G., Crawford, S., Gulbis, A., Barway, S., Zietsman, E., Kotze, M., Buckley, D. A. H., O'Donoghue, D., Siegmund, O. H. W., McPhate, J., Welsh, B. Y., & Vallerga, J. 2011, MNRAS, 416, 2202